Coupling between Progressive Damage, Temperature and Permeability of Concrete: Experimental and Numerical Study

Abdelhafid Khelidj, Marta Choinska, Georges Chatzigeorgiou, Gilles Pijaudier-Cabot

Coupling between Progressive Damage, Temperature and Permeability of Concrete: Experimental and Numerical Study

A. Khelidj[1] , M. Choinska[2], G. Chatzigeorgiou[3] and G. Pijaudier-Cabot[2]
[1]R&DO, Institut de Recherche en Génie Civil et Mécanique, Université de Nantes, Saint-Nazaire, France
[2]Ecole Centrale de Nantes, Nantes cedex 3, France.
[3]Aristotle University of Thessaloniki, Dept. of Civil Engineering, Division of Structures, Thessaloniki, Greece

Abstract

A synthesis of work carried out for several years within our laboratory is presented. The first part includes an experimental study. The tests are performed on hollow cylindrical concrete specimens, subjected to compressive loading. At stress levels lower than 80 % of the peak stress, the variation of permeability is small and it is slightly influenced by the stress, but as the load exceeds 80 % of the peak stress, micro-cracking increases rapidly, causing an increase of the permeability and a greater sensitivity to the applied load. In the post-peak phase the increase of permeability is much larger due to significant crack width growth. The effects of the applied load on permeability are greater with temperature. Finally, the experimental results seem to agree with the format of coupled evolution of the permeability due to damage and temperature assumed by Gawin et al. [10].

The second part of this paper includes a numerical study. The lattice mechanics model is extended to the hydraulic problem and, for this case, it appears that permeability is the size independent variable. Additionally, the evolution of permeability with damage and with stress ratio in the pre-peak phase is compared with experimental results on different types of concrete.

Keywords: Concrete, durability, damage, temperature, permeability, lattice model.

1 Introduction

Transport properties of concrete, like permeability or diffusivity, influence the durability of the concrete structures by controlling the penetration rate of aggressive agents, but also directly if the structure has a tightness role, like nuclear waste storage structures or confinement vessels of nuclear power plants for instance. These structures, during their service life, are subjected to different types of loads (mechanical, thermal, chemical, restrained shrinkage, aging etc...). Generally, service loads are not significant enough to cause an important degradation of structural concrete. However, with time, the degradation accumulates and may lead to micro-cracking resulting in permeability variations. This contribution aims directly at such confinement structures for which it is critical to evaluate their gas tightness and its evolution with time, both in the case where concrete remains in the pre-peak regime (typically in the normal service life) and also when it might reach locally the post-peak regime, e.g. during integrity tests or accidents, where an increase of temperature is also expected (from 20 °C up to 150 °C in the class of integrity tests considered in this paper).

The evolution of the permeability of concrete may be regarded, on one hand, as a function of diffuse micro-cracking in the material (related to damage), and on the other hand as a function of the width, connectivity and tortuosity of newly created flow channels. Relationships between permeability and diffuse damage (micro-cracking) have been derived theoretically. Dormieux and Kondo [1] used homogenisation techniques and similar results are obtained on discrete (lattice) models [2], as it is shown in the second part of this study. Therefore, in the post-peak regime, when a macro-crack has formed in the structure, permeability is governed by Poiseuille flow, crack tortuosity and crack opening (see, e.g. Ref. [3]).

Some experimental results on the interaction between permeability and load induced micro-cracks in uniaxial compressive tests are available in the pre-peak regime. A study of Sugyiama et al. [4] on the effect of a compressive stress on permeability of concrete has shown that the increase of permeability becomes significant when the stress level reaches 75-90 % of the ultimate strength for normal-weight and light-weight concretes. Hearn and Lok [5] observed an important increase of air permeability with load induced micro-cracks, occurring at the critical stress level of 70 % of the ultimate axial compressive strength, and corresponding to the development, and then the interconnection of cracks in the mortar matrix. A study of the residual transport properties of concrete, carried out by Picandet et al. [6], has shown that gas permeability increases exponentially with the axial compressive damage (relative stiffness loss) in the pre-peak phase. Therefore, in the post-peak regime, when a macro-crack has formed in the structure, Brazilian splitting tests, have emphasized a correlation between the water permeability and the crack width as shown in [7].

Modifications of the concrete porosity, which may take place in the range of considered temperatures (from 20 up to 150 °C) are multiple. Among the most important results, the following can be mentioned: modification in moist content due to free water evaporation (up to 105 °C), chemical dehydration of cement paste due to loss of bounded water (beyond 105 °C), thermal expansion, porosity increase, thermal cracking due to thermal and mechanical incompatibility, etc. A considerable increase of gas or water permeability, if measured under temperature or after thermal treatment, has been observed experimentally. Lion et al. [8] found that a thermal treatment of a mortar leads to an increase of residual porosity and gas permeability, being sevenfold its initial value (measured at 25 °C) after a treatment at 250 °C. The tests performed by Joos and Reinhardt [9] emphasized an increase of water permeability of 10-14 % between 20 °C and 50 °C, and of 7-11 % between 50 °C and 80 °C, almost the amount of what could be predicted according to theoretical considerations based on thermodynamics [9]. According to Gawin et al. [10] a power relationship between temperature and concrete permeability should be considered.

Existing experimental data provide some correlation between the material mechanical degradation (micro-cracking and macro-cracking) and the permeability of concrete. The same exists for the influence of temperature on permeability of concrete but very little data is available on the coupled temperature and load effects on the permeability of concrete. At the same time, theoretical results or phenomenological formulas exist in both cases but then again, the interaction between the applied load and the temperature on the material permeability lacks experimental validation. Therefore, the objective of this paper is to provide experimental data from which such validations can be carried out. Because of the specific application aimed at this study,

maintenance of nuclear confinement vessels and service life evaluation, we need to consider at the same time variations of permeability due to moderate damage (homogenously diffused microcracks developing in the pre-peak phase) and localized one (macrocrack(s) localizing and propagating in the post-peak phase).

In the first part of the current paper the experimental device and the testing procedure are first presented. Then, the results of the experimental study are shown and discussed.

The second part includes a numerical study. We suppose that concrete is a disordered material, which we can simulate with the help of a simple discrete lattice model. In the previous study it has been shown that the evolution of Young modulus is a variable which tends to be independent from the size of the lattice until the peak load. In this paper we extend the model for the hydraulic problem and, for this case, we can see that permeability is the size independent variable. Finally, the evolution of permeability with damage and with stress ratio in the pre-peak phase is compared with experimental results on different types of concrete.

2 Experimental Program

2.1 Concrete Composition and Specimen Curing

An ordinary concrete of water to cement ratio equal to 0.6 with maximum aggregate size of 16 mm is used. The cylindrical (110x220 mm^2) hollow specimens have been cast in metal moulds. A cylindrical borehole was cast in each specimen by placing a metallic bar (diameter of 14 mm) in the moulds. All the specimens have been subjected to the same curing and conditioning processes. They were stored in water during 28 days and dried in a ventilated oven initially at 80 °C (28 days), then at 105 °C down to constant mass. The dry state has been also maintained during the permeability tests whenever possible using the climatic chamber.

The average mechanical response of concrete in uniaxial compression is shown on Figure 1: after the storage in water (at 28 days), after drying at 80° C (at 2 months) and 105 °C (at 4 months). Average mechanical properties are provided in Table 1.
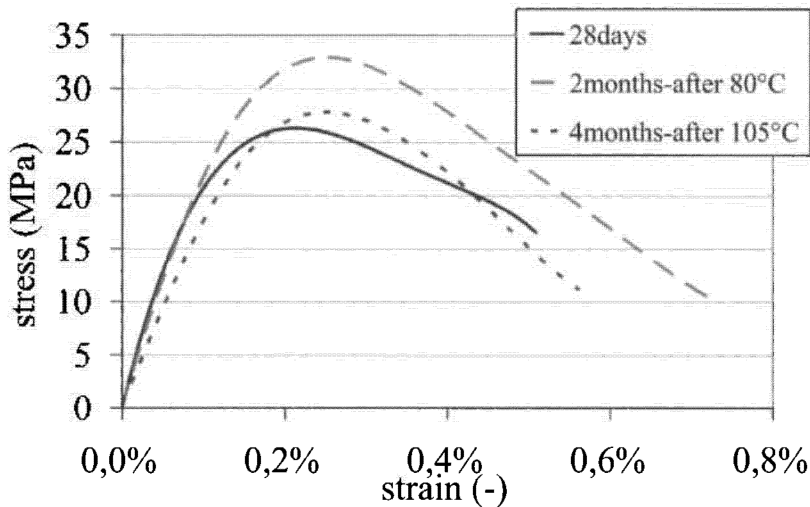
Figure 1: Stress-axial strain curves of tested concrete (at ambient temperature)

Table 1: Mechanical properties of the concrete

	28 days (wet cure)	4 months (after drying)
Modulus of elasticity (GPa)	23	16
Peak stress (MPa)	26	28
Axial peak strain (-)	2,2.10^{-03}	2,6.10^{-03}

2.2 Application of Requested Thermal and Mechanical Loading

A specimen, placed in a climatic chamber, is loaded in a simple compression test. The climatic chamber generates and controls temperature and relative humidity. Three levels of temperatures are used: 20 °C, 105 °C and 150 °C. In this study relative humidity is maintained close to 0 % in order to keep material dry . However, the tests on different saturation levels can be carried out with this device. The compression tests are performed with a hydraulic loading frame MTS 500 kN under displacement control. The specimen is placed between two metal platens designed to apply the compressive force and to enable at the same time the injection of the percolating fluid. The axial contraction of a specimen is monitored by three linear variable displacement transducers (LVDT) placed on the circumference of the specimen. The axial contraction of the specimen is monitored by three linear variable displacement transducers (LVDT) placed on the circumference of the specimen.

2.3 Gas Permeability Measurements

Presented permeability tests are performed within the framework of the steady state gas flow in isothermal conditions. The principle of gas permeability measurement during loading is given on the simplified diagram on Figure 2.

Inert gas (nitrogen), with respect to concrete, is injected into the cylindrical borehole through the perforated bottom platen. Due to the tightness of the two faces of a hollow cylindrical specimen, the obtained gas flow is radial. A relative pressure P_i-P_{atm} (difference between applied absolute pressure and atmospheric pressure) is applied and maintained till the gas flow stabilization through the specimen. Pressure values and flow rates are measured at the upstream of the specimen. The flow equation and mass balance equation lead to the determination of a gas permeability coefficient k_a [m^2]. The permeability coefficient, called subsequently permeability, is calculated from equation (1), which corresponds to the Hagen-Poiseuille's law adapted for gas laminar flow through a porous body. When the injection flow rate Q_i [m^3/s] is known, the permeability k_a [m^2] can be calculated:

$$k_a = \frac{Q_i \cdot P_i \cdot \mu \cdot \ln\left(\frac{r_2}{r_1}\right)}{\pi \cdot H \cdot \left(P_i^2 - P_{atm}^2\right)} \qquad (1)$$

where

P_i [Pa] is the applied absolute pressure at the upstream, P_{atm} [Pa] is the atmospheric pressure at the downstream, μ [Pa.s] is the dynamic viscosity of gas (nitrogen); r_1 [m], r_2 [m], H [m] are the inner and outer radius and the height of the cylindrical specimen respectively.

This permeability is relative to the overall gas flow through the material, consisting of the viscous flow and the slip flow (Knudsen effect). The slip flow appears when the average diameter of the capillaries crossed by gas is of the size of the mean free path of the gas molecules (average distance between collisions).

During mass transport through concrete, the contribution of slip flow in the overall gas flow may be very significant. Hence the permeability, determined for different gas pressures, depends (among other factors due to the microstructure of the material) on the pressure and the temperature, factors which influence the mean free path, which is inversely proportional to the pressure. The permeability k_a is apparent. In order to get an intrinsic per-
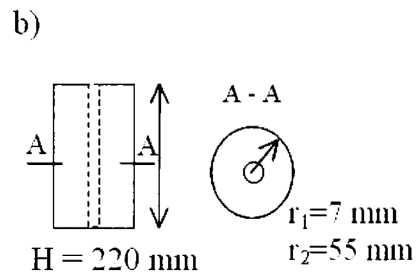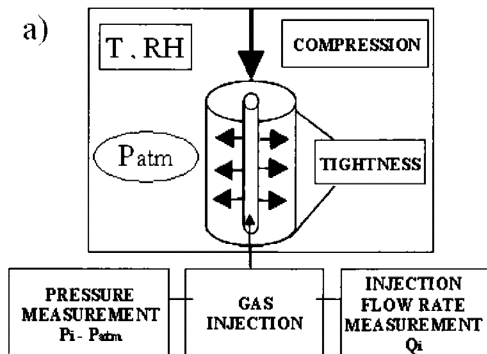

Figure 2: a) Simplified diagram of the experimental device   b) Geometry of the specimen

meability, a characteristic of the porous medium solely and being strictly relative to the viscous flow, Klinkenberg or Carman approach may be applied. In this study the relationship due to Klinkenberg [11], presented in equation (2), is used:

$$k_a = k_v (1 + \frac{\beta}{P_m})$$ (2)

where

P_m [Pa] corresponds to the average gas pressure,

$$P_m = \frac{P_i + P_{atm}}{2}$$

and β [Pa] is the Klinkenberg coefficient, a constant which is inversely proportional to the average diameter of the capillaries. The intrinsic permeability k_v [m^2] is obtained by extrapolating the apparent gas permeability k_a determined at various pressures to the case of an infinite pressure.

2.4 Experimental Procedure

Prior to the test a specimen is removed from the drying oven and is left in a desiccator placed in a air-conditioned room (20 °C) for 48 hours. After this period, a specimen instrumented with the displacement transducers (LVDT) and positioned in the permeability cell between the platens of the hydraulic press. This setup is then enclosed in the climatic chamber (Figure 3).

During the tests, the measurements of the apparent permeability are performed for five relative pressures: 0.3, 0.25, 0.20, 0.15, and 0.10 MPa. Afterwards, the intrinsic permeability is determined

according to the Klinkenberg relationship (2). The upstream mass flow rate is given by one of the three digital thermal Mass Flow Meters (MFM) of ranges: 10-500 ml/min, 20-1000 ml/min, and 300-15000 ml/min respectively. A period of 2 to 5 minutes approximately, is necessary in order to reach the steady state gas flow. During the test, the applied force, the stroke displacement, the displacements measured from the LVDTs, the gas pressure and mass flow rate through the specimen are recorded. The accuracy of measurement of the apparent permeability is 2 % approximately. The full testing procedure is as follow:

- First, a measurement of the *initial permeability* of concrete is performed at 20 °C, with an axial compressive load of 4 kN, resulting in the compressive stress of 0.4 MPa (negligible stress for this concrete). This load ensures the fitting between the specimen and the load platens. It is needed for ensuring the tightness of the permeability cell (radial flow only).
- Then, the required temperature is applied (20 °C, 105 °C or 150 °C). During heating at a constant rate of 5 °C/h, the compressive load of 4 kN is kept. A stabilization period of temperature through the material is needed, thus permeability tests start after 60 hours, under a constant temperature. Prior to that, the *reference permeability* is measured again in order to obtain the effect of the temperature.
- Afterwards, the specimen is loaded with a displacement rate of 0.02 mm/mn up to the required load level. Load levels correspond to 20, 40, 60, 80 and 90 % of the estimated peak stress in the pre-peak regime, while close to
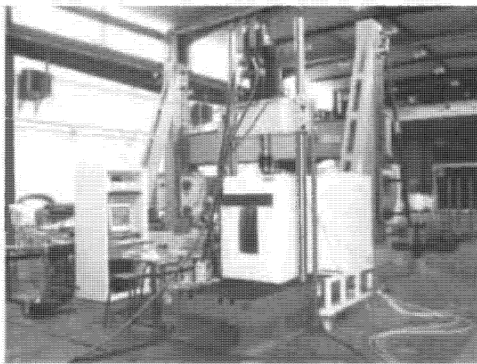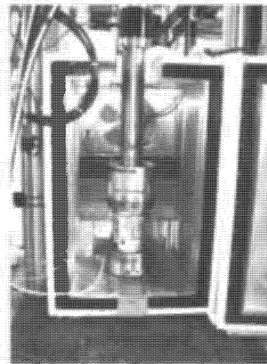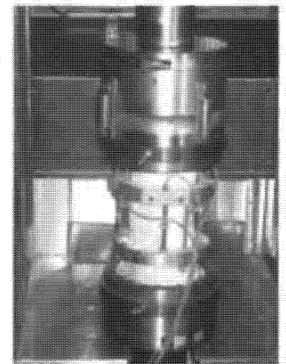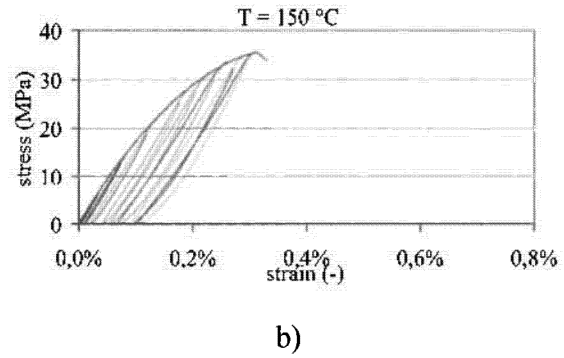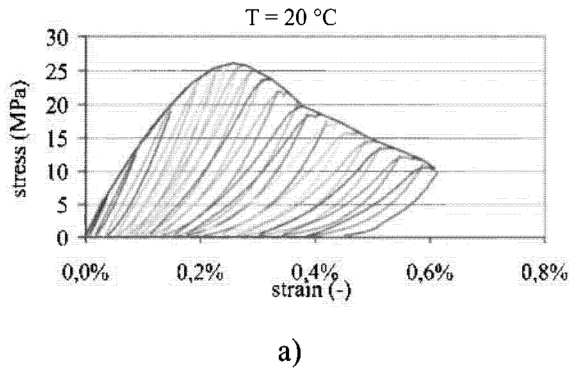

a)   b)   c)

Figure 3: Test configuration a) Overall view b) Temperature device c) Mechanical set-up (LVDTs) and permeability cell.

Figure 4:   a) Typical stress-strain relation at 20 °C   b) Typical stress-strain relation at 150 °C

the peak and in the post-peak phase each load level corresponds to an increase of axial strain of 0.3 mm/m. Each load level is maintained during 30 minutes in order to allow for the determination of the gas permeability. For each load level, once the permeability under load (*loading permeability*) is measured, the specimen is unloaded down to 4 kN and the permeability of the unloaded specimen is measured (*unloading permeability*).

Time dependent effects (creep or relaxation) are not significant during the pre-peak phase. Nevertheless, close to the peak and beyond, the flow rate measurements are affected by load relaxation. In this case, the time needed to reach a steady state flow rate raises and corresponds to the stabilization of cracks propagation for the imposed displacement, which is kept constant. All the results presented below refer to the values of permeability obtained with a minimum of three tests per temperature.

3   Results and Discussion

The initial permeability of the concrete tested (prepared with three batches) vary between 6.10^{-17} m² and 12.10^{-17} m². This variation according to casting is thus relatively small and illustrates the good reproducibility of the test results. Besides, the initial permeability is overestimated due to the drying-shrinkage cracking [12], increasing the gas permeability. The main intention of a study is, although, to examine permeability evolution as a function of mechanically induced cracking and temperature, so that the initial permeability values remain only a referential state.

Experimental results obtained on tested concrete revealed a consistent temperature dependent behaviour, getting more and more brittle with tempera-

ture and tending to brittle fracture.The typical stress-strain responses recorded during the tests carried out at 20 °C and 150 °C are presented in Figure 4. Unfortunately, the brittle behaviour at 150 °C restricts permeability measurements in the post-peak phase.

3.1   Permeability under Loading and after Unloading

The results presented in Figure 5 show the permeability measured under applied load and after unloading for different maximum applied stress levels at 20 °C and 150 °C (only 2 tests per temperature are presented for the sake of clarity of the plots). An average relative difference between permeability measured under applied load and after unloading of 5 % at 20 °C, of 6 % at 105 °C and of 18 % at 150 °C is observed. It can be noticed that for low and intermediate maximum applied stress levels, the permeability measured after unloading is slightly greater than during loading. For high maximum applied stress levels, beyond a threshold corresponding to 80 % of the peak stress at 20 °C, and close to 90 % at 105 °C and 150 °C, the inverse trend is observed.

This effect is remarkable not only on the intrinsic permeability (calculated from Klinkenberg relationship), but also on the apparent permeability (Figure 6). Apparent permeabilities, measured during loading for a moderate stress level (19 % of the peak stress) at any average pressure of gas injection, are lower than after unloading; while for a significant stress level (91 % of the peak stress) the result is opposite.
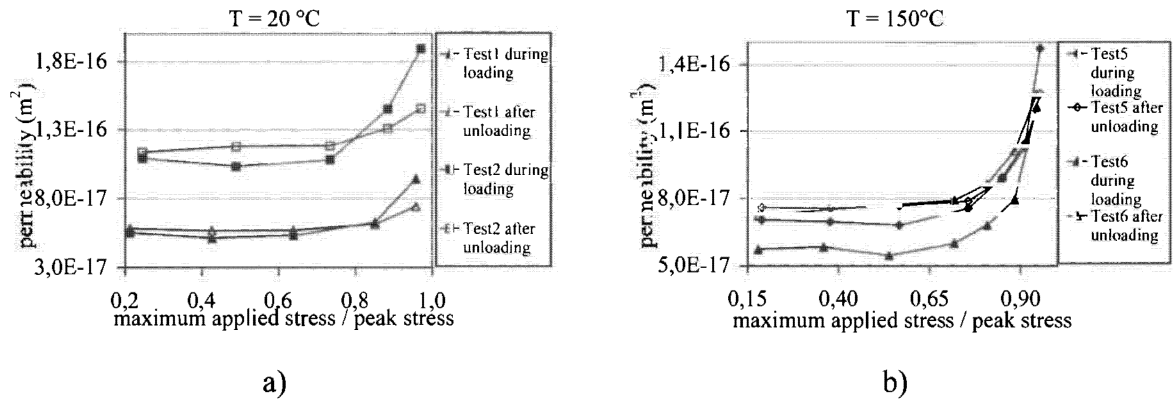
Figure 5: Loading and unloading intrinsic permeability vs maximum applied relative stress at a) 20 °C b) 150 °C.
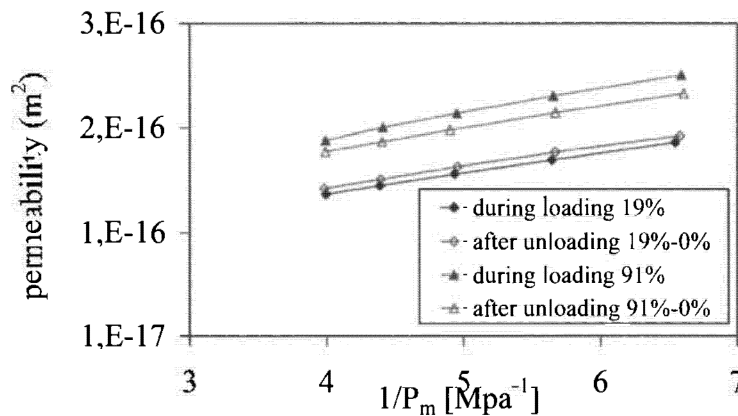
Figure 6: Effects of loading and unloading and of the mean gas pressure on the apparent permeability values (typical result, at 20 °C).

The ratio of loading to unloading permeabilities varies with the applied stress level and temperature. In the strain space (longitudinal strain), it may be represented by a function which is negative in the early pre-peak phase, reaches a maximum in early post-peak phase for a relative strain equal to 1.1-1.2 (maximum load induced strain to peak strain), and tends to become a constant further in the post peak regime (the two permeabilities are equal). This relation is plotted in Figure 7 for the three tested temperatures.

Low compressive stress levels act on the initial porosity by squeezing it (volume contraction), which yields a decrease of permeability. In this phase, unloading generates the opposite effect and thus the permeability increases (the behaviour is reversible). Till approximately 60-70 % of the peak stress at 20 °C and till 70-75 % of the peak stress at 105 °C and 150 °C, the permeability measured after unloading remains quasi-constant, while the per-

meability measured during loading slightly decreases (Figure 5). Possible micro-crack formation is compensated by the closure of existing pores and the resulting effect on the permeability is a slight decrease. Upon unloading, cracks induced by the applied load may close while existing pores or cracks open again, with an increase of the permeability. Beyond these stress levels, permeability measured during loading exceeds the values revealed after unloading. The amount of micro-crack formed is enough in order to compensate effect of closure of the initial microstructure. Consequently, the permeability measured during loading reaches greater values than after unloading.
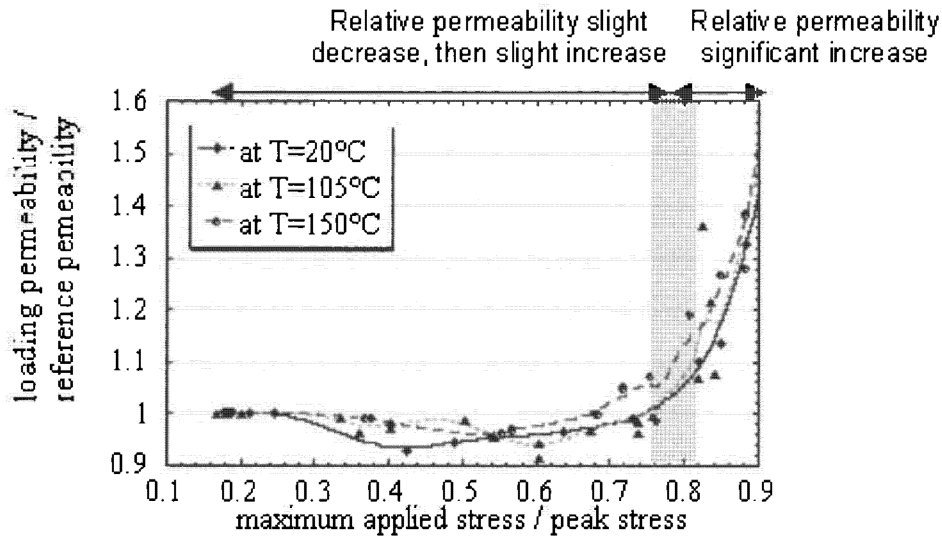
3.2 Pre-Peak Phase

3.2.1 Permeability Variation under Mechanical Loading

In the pre-peak phase, for each temperature (20, 105, 150°C), the characteristic phases of relative
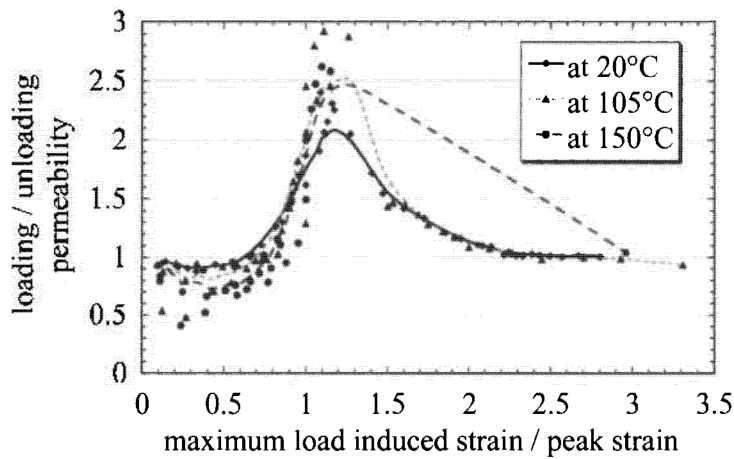
Figure 7: Loading to unloading intrinsic permeability ratio vs applied relative strain
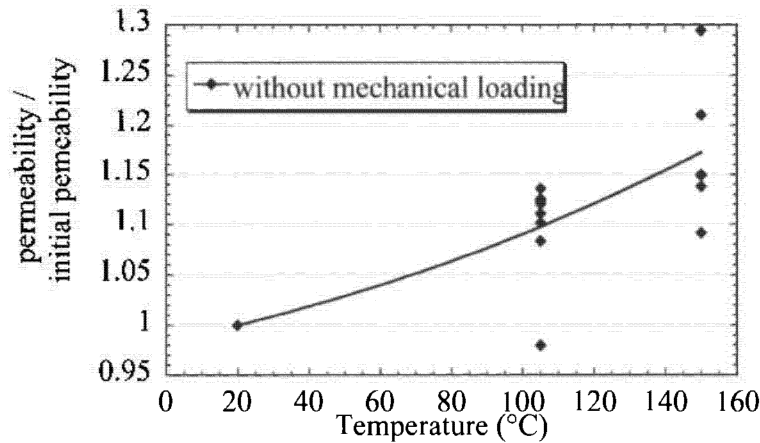

Figure 8: Variation of intrinsic permeability values with loading for tested temperatures

permeability evolution (permeability at temperature of 20, 105 or 150 °C over the reference permeability at temperature of 20, 105 or 150 °C, respectively) can be distinguished, as it is shown in Figure 8. Here, results consider the intrinsic permeability measured during loading only.

Under the action of low and intermediate load level, corresponding to 40-60 % of the peak stress, the permeability tends to decrease slightly. Beyond this load level the permeability increases, first very slightly, then significantly, with the most important rate for the test carried out at 150 °C.

The relative permeability evolution during loading, joining up with previously presented results, is

related to volumetric behavior of concrete under uniaxial compression. Therefore, it can be considered, that the slight decrease of the permeability for low load levels (Figure 8) is due to contracting volumetric behavior under uniaxial compression. However, at 68-74 % of the peak stress, the permeability regains its initial value, before more important increase. Therefore, when volumetric behavior becomes definitely dilating, the permeability increases first slightly, due to the development of homogenously diffused microcracks through the cement paste, then significantly due to the microcracks coalescence (from 80 % of the peak stress, corresponding to the transition in volumetric

Figure 9: Variation of intrinsic permeability under temperature. Measures carried out under thermal loading.

behaviour [4]). Therefore, for the three tested temperatures, at stress levels lower than 80 % of the peak stress, the permeability variation is insignificant but, as the load exceeds 80 % of the peak stress and approaches the peak stress, the damage increases rapidly causing a significant change in the permeability. This change seems to be greater with the increase of temperature. It can be explained by the fact that more brittle concrete with temperature (or with other parameter) is, more the cracks will localize, and thus the rate of permeability evolution will be greater.

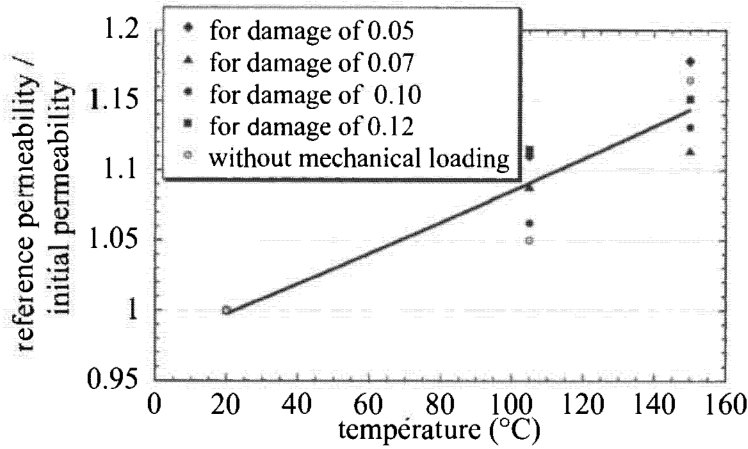### 3.2.2 Permeability Variation under Temperature

An increase of the relative permeability with temperature is observed in Figure 9 (permeability measured at 20 °C, 105 °C or 150 °C over the initial permeability measured at 20 °C).

Several reasons for the slight increase of permeability with temperature might be considered. Between 20 °C and 150-200 °C, thermal expansion of the cement paste and aggregates takes place [8]. Because the thermal expansion coefficients are different for each constituent of concrete, micro-cracks should appear at the cement paste-aggregate interface. Beyond 150-200 °C, the expansion of the aggregates is limited by the shrinkage of the cement paste, what results in cracking through the latter. In this range of temperatures the cement paste shrinks due to dehydration. Therefore, chemical bonds, forming the CSH gel, start to break down. Hydrated products transform into anhydrous product and free water evaporates during further heating and creates new channels

accessible for the gas flow. Furthermore, porosity and pores distribution change, due to the exposure to high temperatures, has already been emphasized by experimental evidences, as reported in [13].

In our study, the increase of relative permeability observed at 105 °C compared to 20 °C cannot be related to thermal micro-cracking. This temperature has already been experienced by all the specimens during drying. Since moisture effects cannot occur, one remaining cause is the widening of pores through relative thermal expansion of the (heterogeneous) material. In order to verify this assumption, the microstructure of the material needs to be scrutinised. One useful indication, serving as a first step in such a study, is the analysis of the variation of the Klinkenberg coefficient β [Pa]. It is inversely proportional to the average diameter of the pores and thus it may be considered as an indicator of the fineness of the porosity in the material. A decrease of β of 10 % is observed between 20 °C and 105 °C. This decrease is related to the increase in the pore size, which takes place due to the thermal expansion of the porous material. Consequently, the intrinsic permeability increases most probably due to the pores widening between 20 °C and 105 °C.

The increase of permeability at 150 °C, compared to the two other levels of temperature has to be likewise related to pores widening. However, a decrease of β has not been observed in the tests; on the contrary, an increase (of 30 %) of β has been computed. It means that the contribution of very fine pores, created by the thermal treatment at 150 °C, is relatively more important than pores widening at this temperature.

a)
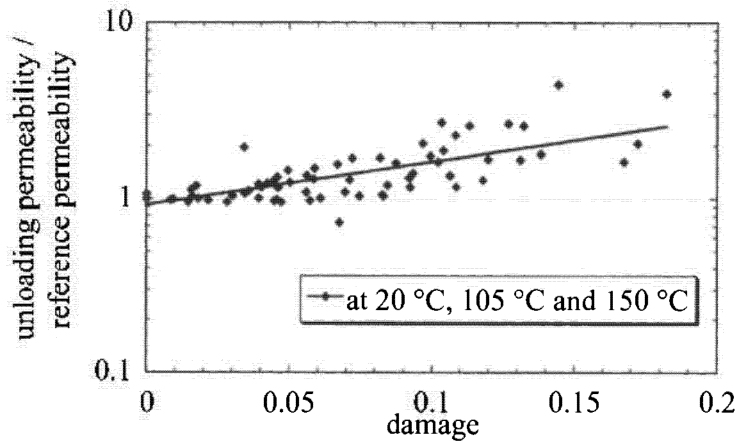
b)

Figure 10: a) Variation of relative intrinsic permeability with temperature for the damage levels b) Variation of relative intrinsic unloading permeability with damage for the three tested temperatures.

3.2.3 Permeability Variation with Damage and Temperature - Interaction Law

Apart from the separate effect of the mechanical load and temperature on the permeability, some information can be obtained as far as the coupled effect of load and temperature on permeability is concerned:

First, the effect of the temperature on the permeability has been measured with applied mechanical load. This is shown in Figure 10 a) for some damage levels. Effectively, the evolution of the permeability with the temperature is almost the same for any damage considered.

Following the analysis by Picandet et al. [6], it is more consistent, in the pre-peak phase to record the evolution of the permeability with damage instead

of the strain or stress. In order to analyse the effect of the applied load on permeability we follow here the same procedure and compute damage from the variation of the unloading stiffness recorded on the mechanical response of the specimen. The result is shown in Figure 10 b). On this plot, we have the permeability evaluated after unloading as a function of damage d defined as

$$d = \frac{E_0 - E_{unloading}}{E_0}$$

where E_0 is the initial Young's modulus of the material and $E_{unloading}$ is the unloading modulus. Same as in [6], the plot exhibits some dispersion due to the evaluation of the unloading slopes. Still, the agreement for all the temperatures seems cor-

rect. One may say that the evolution of the permeability due to the applied load for the three temperatures tested falls on the same master curve. Note that we have considered in this figure the permeability measured after unloading instead of the permeability measured under load, since it is expected that on top of the first one, some load effect could be accounted for, or possibly neglected in the pre-peak regime (for conservative safety reasons, the decrease of permeability may be neglected).

Therefore, one may possibly say that the overall evolution of the permeability follows a multiplicative format:

$$k = f(damage) \cdot g(temperature)$$

The increase of permeability due to temperature and damage is the product of two functions (f and g) which reflect each contribution separately. Our experimental results are also consistent with the formula proposed by Gawin and co-workers [10].

3.3 Peak and Post-Peak Phases

The results presented in Figure 11 show the complete evolution of the relative permeability during loading and after unloading with the maximum applied relative strain for the three tested temperatures. It turns out that at the peak (relative strain equal to 1), permeability tends to tenfold initial value, if measured during loading at elevated tem-

peratures (105 °C and 150 °C), and up to fivefold, if measured at 20 °C. Therefore, up to the peak, relative permeability change is quite temperate in comparison with the behavior in post-peak phase, where the change becomes tremendous (several orders of magnitude) due to significant cracks width increase. Consequently, the fluid flow through damaged concrete is controlled by the opening and connectivity of cracks.

However, it is still observed that permeability rate increases with temperature. At 105 °C, though this temperature was submitted by the concrete during drying, the change in permeability is greater, than at 20 °C. For the tests carried out at 150 °C, due to high brittleness of concrete at this temperature, permeability could not been measured in the post-peak phase. Some experimental results, presented in Figure 11 for 150 °C, correspond to permeability measured at failure. Moreover, it comes into light that permeability varies with different kinetics in function of temperature in the strain space. Beyond relative strain equal to 1, two regimes of permeability variation are manifested for all tested temperatures: the first one (up to 1.5 of relative strain), where permeability increases rapidly and the second one, which is characterized by a steady and less rapid rate. Indeed, flow localization, following damage localization, should hither occur. These observations are in qualitative agreement with the results obtained by Wang et al. [7].
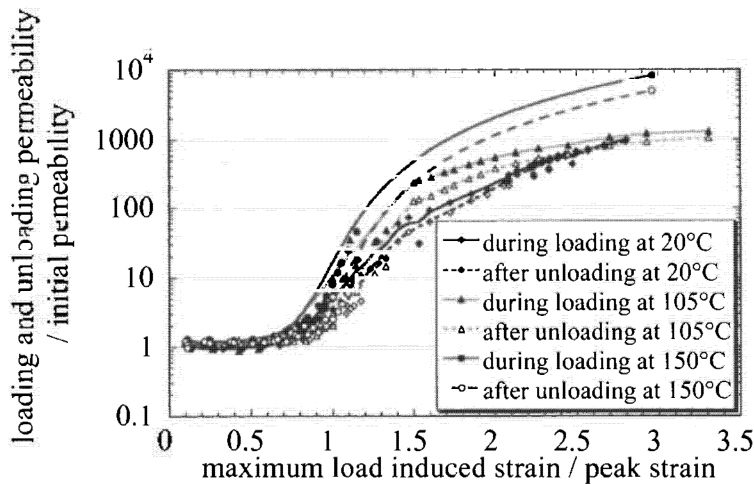
Figure 11: Variation of relative intrinsic permeability with maximum applied relative strain for the three tested temperatures. Measurements carried out at temperature, during loading and after unloading
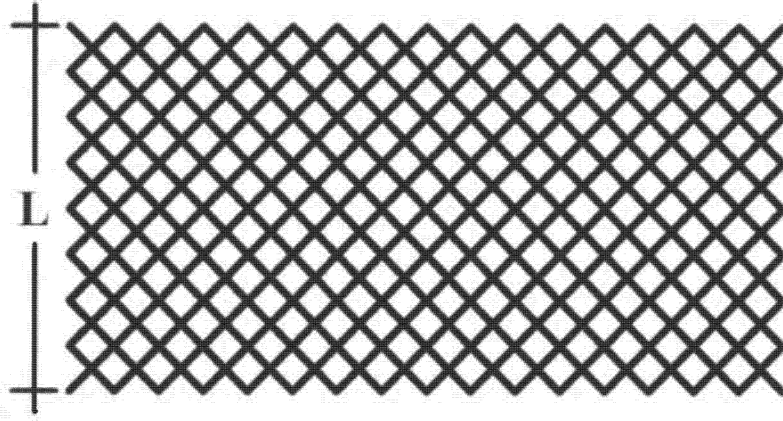
Figure 12: Lattice model

4   Numerical Study

Aim of this study is to examine the relation between the mechanical damage and the permeability of concrete. Assuming that concrete is a disordered material, we can simulate it with the help of a simple, stiffness controlled, discrete lattice model. The model was used [14] in the past for the study of the failure mechanism of quasi-brittle materials. In the lattice, the mechanical problem is substituted by an electrical analogous, simplifying with this way the analysis, by transforming it from vectorial to scalar.

As De Arcangelis et al. [15] have shown, this simplification is able to capture the most important physical aspects of the problem. In this electrical analogous, the strain is substituted by the voltage difference, the stress by the current and the Young Modulus by the conductance. As it is depicted in Figure 12, the model is a regular two-dimensional lattice whose bonds are one-dimensional.

The boundary conditions of the model are periodic, in order to attain the creation of an infinite system and the partly avoidance of the boundary effects. They represent a homogeneous loading in the vertical direction: Periodicity is imposed along the boundaries parallel to vertical axis and a constant jump in voltage is applied along the two horizontal boundaries. Every bond of the lattice behaves as a brittle material with a conductance equal to 1. When the current of a bond reaches a threshold current, the bond fails. This threshold differs from bond to bond, following a uniform random distribution between 0 and 1. With this way, we ensure the disorder of the model and, consequently, the heterogeneity of the material.

The calculation process starts by assigning a threshold current to every bond with the help of a random generator number [16]. At each step, the algorithm computes the voltage at each node from Kirchhoff's law. The equations form a symmetric band matrix which can be solved using Cholesky factorization. From Ohm's law, the current of each bond is obtained. The bond which fails first is the one with the minimum ratio of its strength (threshold current) to its current. This bond is removed from the lattice, by changing its conductance from 1 to 0. Because the analysis is linear, it is also possible to compute the overall load at which this bond fails and the process continues with the next step of loading, where we seek for the next bond which fails.

The lattice does not represent a real material. In fact, we are interested in its scaling properties: as the lattice size tends to infinity, its response tends to a thermodynamic limit which is the response of a single point in a continuum approach. Hence, we shall look at the variables that are capable of describing the evolution of the lattice response with bond failure, independently from its size. For the characterization of the distribution of local stresses, we introduce the concept of moments, which are given by the expression:

$$M_m = \int i^m N(i)\,di \qquad (3)$$

where i is the current of each bond, N(i) is the number of bonds whose current is in the range of [i, i+di], and m is the order of moment. The most important moments are these of order up to 4, because of their physical meaning: moments of order 0 represent the number of unbroken bonds in the lattice, moments of order 1 the average stress,
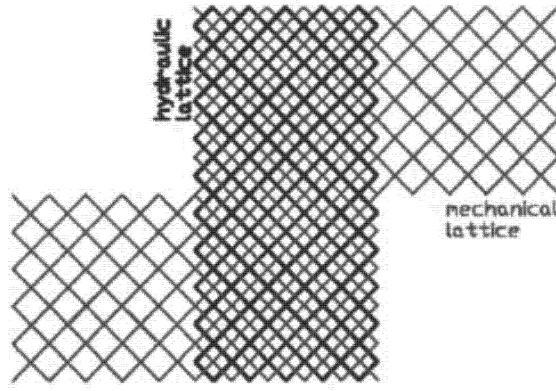
Figure 13: Mechanical and hydraulic lattices

moments of order 2 the average Young Modulus and moments of order 4 the dispersion of the Young Modulus.

As each lattice has a unique distribution of bond thresholds, several computations with different random seeds (following a uniform distribution) and different lattice sizes must be performed. With this way we obtain a representative statistical treatment of the results, which provide us useful conclusions about the average behaviour of the lattice.

Summarizing the major results of the mechanical analysis, we recall that the average of the Young modulus, and not the number of broken bonds, is a lattice size independent parameter, i.e., the continuous variable which captures, in a continuum sense, the evolution of damage. Moreover, the post-peak area seems to be strongly lattice-size dependent, a fact that was expected from experimental evidences. For the hydraulic problem, we use the lattice analysis in order to investigate the relation between the permeability and the cracking mechanism. More details about this study can be found in Chatzigeorgiou et al.[2]. In this analysis, we use a lattice perpendicular to the mechanical one (figure 13), and solve for the hydraulic problem, assuming that, when a bond fails in the mechanical problem, the bond that is perpendicular in the hydraulic problem increases its permeability from 1 to a large value K. Now, the physical meaning of the moments is different: moments of order 0 represent the number of unbroken bonds, moments of order 1 the average flow rate, moments of order 2 the average permeability and moments of order 4 are a measure of the dispersion of the permeability.

From the corresponding moment distributions in the hydraulic problem we find that, the variable that
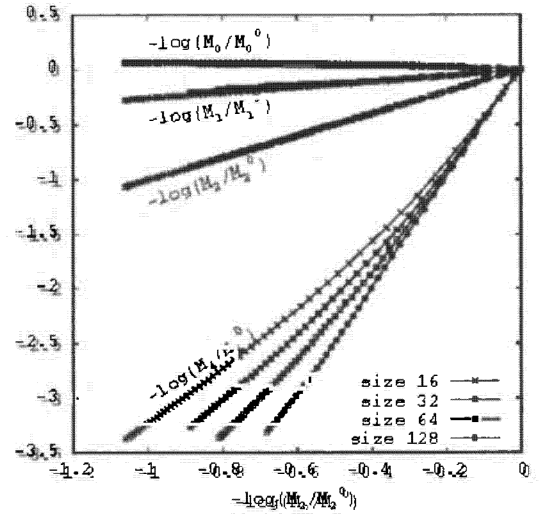
**Figure 14:** Hydraulic moments vs. M_2 until peak load
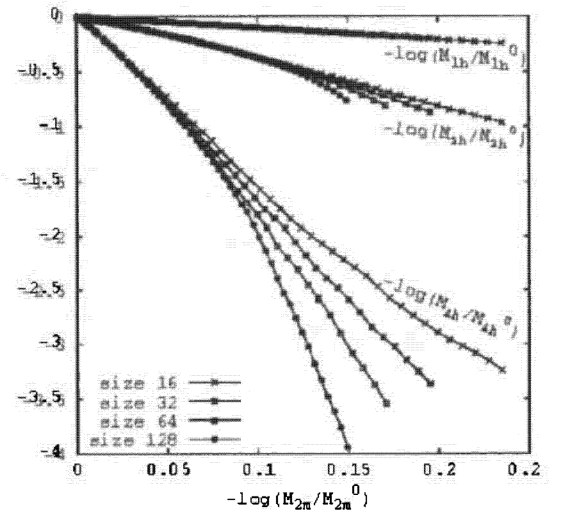
Figure 15: Hydraulic moments vs. M_{2m} until peak load

is independent of the lattice size is the average permeability (Figure 14).

We also observe that the average Young Modulus (M_{2m} in figure 15) is able to describe the hydraulic problem independently of the lattice size. This suggests that in a continuum model, the permeability should increase with damage.

From Figure 16, we see that the average permeability of lattice increases rapidly, as the loading approaches the maximum stress. This is in agreement with what Sugiyama et al.[4] have observed.

Figure 17 shows the evolution of the permeability as a function of the evolution of stiffness (mechani-
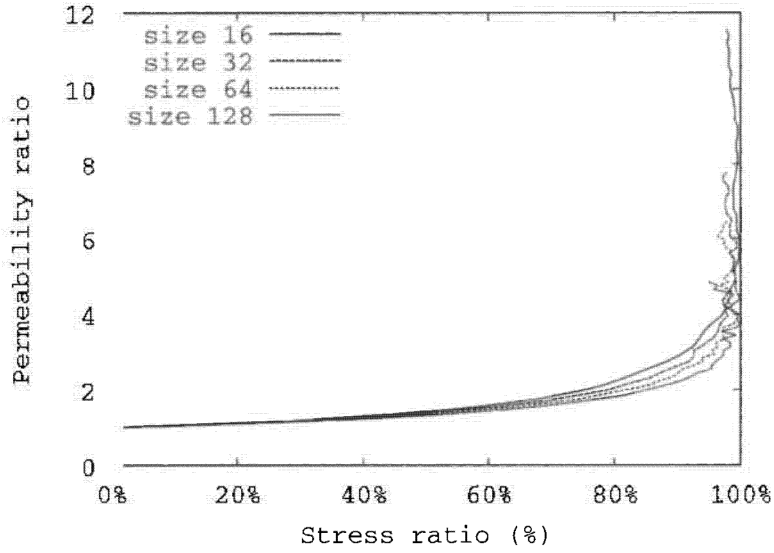
Figure 16: Permeability vs. stress ratio
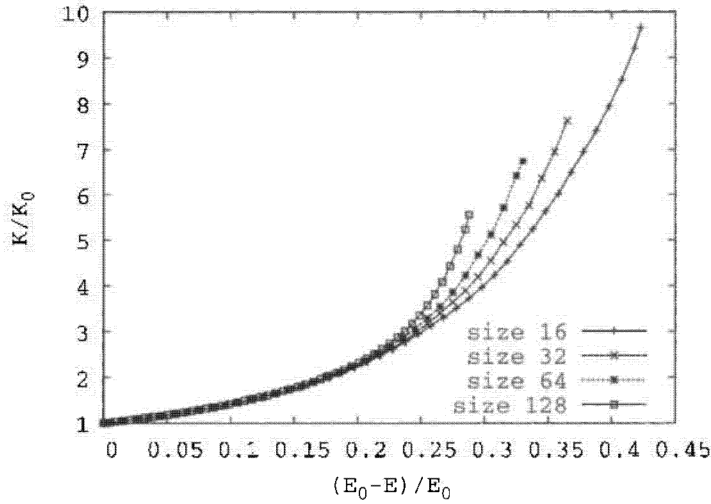
Figure 17: Permeability vs. mechanical damage

cal damage) in the mechanical lattice. We observe that for stiffness variations between 0 and 0.2, the plots collapse onto the same curve. Picandet et al. [6] have shown that the permeability versus mechanical damage curve is the same for three different types of concretes. So the lattice analysis seems to agree with the experimental observations, which show that there must be an intrinsic relationship between the permeability and the evolution of the material stiffness.

5 Conclusions and Perspectives

The results reported in the first part of this paper can be summarised as follow:

- In the pre-peak phase, at stress levels lower than 80 % of the peak stress (i.e. common stress levels in a real structure), the variation of permeability is small and it is slightly influenced by the stress. As a matter of fact, the permeability under load is smaller than the permeability measured after unloading.

- As the load exceeds 80 % of the peak stress (i.e. exceptional stress levels in a real structure), micro-cracking increases rapidly, causing an increase of the permeability and a greater sensitivity to the applied load, i.e. a noticeable difference between the permeability measured under load and after unloading, the first becoming greater than the latter.

- In the post-peak phase an important growth of permeability takes place due to the crack widths growth under compressive loading. The change of permeability seems to be greater with the increase of temperature.

- The permeability increases with the temperature. At 105 °C (temperature already experienced by the material previously) it is due to the pore widening due to thermal expansion of concrete porous material. At 150 °C, where the increase is much more important, it is due to pore widening and temperature induced micro-cracking.

Finally, the experimental results seem to agree with the format of coupled evolution of the permeability due to damage and temperature:

$$k = f(damage) \cdot g(temperature)$$

assumed by Gawin et al. [8]. Obviously, this is not a general proof that the above relationship should hold for any temperature or damage, but experimental data are not in contradiction with it. Further studies with a wider range of temperature are needed in order to judge the validity of this assumption in a more general context.

The hydro-mechanical problem is also analysed by construction of a sister lattice to the mechanical one. When a bond breaks in the mechanical lattice, it increases the permeability of a bond in the hydraulic lattice that is perpendicular to the first one. The analysis of the lattice results follows the technique implemented in the mechanical problem. The various moments of the flow rate distribution are computed and we look for the variable that describes the evolution of these moments independently from the size of the lattice. If such a quantity is found, it is the quantity that describes the evolution of the flow rate distribution with material degradation.

The permeability of the lattice increases progressively with the increase of material degradation. The average permeability constructs lattice size-independent relations with the hydraulic

moments of order up to 4, for a moderate material degradation, before the peak load is reached. Finally, the combination of the mechanical and hydraulic analyses was examined. The compliance versus hydraulic moment curves are lattice size independent and consequently the plot of the permeability versus the evolution of damage exhibits the same property. It indicates that in continuum poro-mechanics, the material permeability should be related to the degradation of stiffness (damage). This is consistent with the experimental data presented in this paper.

Acknowledgement

References

1. L. Dormieux and D. Kondo, Approche micromécanique du couplage perméabilité-endommagement, C.R. Mecanique 332 (2004) 135-140 (in french).

2. G. Chatzigeorgiou, V. Picandet, A. Khelidj, G.Pijaudier-Cabot, Coupling between progressive damage and permeability of concrete: analysis with a discrete model, Int. J. Anal. Meth. Geomech. 29 (2005) 1005-1018.

3. F.A.L. Dullien, Porous Media. Fluid Transport and Pore Structure, Academic Press (1979).

4. T. Sugiyama, T.W. Bremner, T.A. Holm, Effect of Stress on Gas Permeability in Concrete, ACI Materials Journal 93 (1996) 443-450.

5. N. Hearn and G. Lok, Measurement of Permeability under Uniaxial Compression-A Test Method, ACI Materials Journal 95 (1998) 691-694.

6. V. Picandet, A. Khelidj, G. Bastian, Effect of axial compressive damage on gas permeability of ordinary and high-performance concrete, Cement and Concrete Research 31 (2001) 1525-1532.

7. K. Wang, D.C. Jansen, S.P. Shah, A.F. Karr, Permeability study of cracked con-

crete, Cement and Concrete Research 27 (1997) 381-393.

8. M. Lion, F. Skoczylas, Z. Lafhaj, M. Sersar, Experimental study on a mortar. Temperature effects on porosity and permeability. Residual properties or direct measurements under temperature, Cement and Concrete Research (2005), in press.

9. M. Joos and H.W. Reinhardt, Permeability and diffusivity of concrete as function of temperature, Cement and Concrete Research 32 (2002) 197-1504.

10. D. Gawin, F. Pesavento, B.A. Schrefler, Modelling of hygro-thermal behaviour of concrete at high temperature with thermo-chemical and mechanical material degradation, Comput. Methods Appl. Mech. Engrg. 192 (2003) 1731–1771.

11. L.J. Klinkenberg, The permeability of porous media to liquids and gases, American Petroleum Institute, Drilling and Production Practice (1941) 200-213.

12. N. Hearn, Effect of shrinkage and load-induced cracking on water permeability of concrete, ACI Materials Journal 96 (1999) 234-241.

13. S. Dal Pont and A. Erlacher, Numerical and experimental analysis of chemical dehydration, heat and mass transfers in a concrete hollow cylinder submitted to high temperatures, International Journal of Heat and Mass Transfer 47 (2004) 135-147.

14. A. Delaplace, G. Pijaudier-Cabot, S. Roux : Progressive damage in discrete models and consequences on continuum modeling. Journal of Mechanics and Physics of Solids, vol. 44, No. 1, pp. 99-136. (1996)

15. L. De Arcangelis, H. J. Herrmann : Scaling and Multiscaling Laws in Random Fuse Networks. Physical Reviews B, vol. 39, No. 4, pp. 2678-2684. (1989)

16. W.H. Press, A.S. Teukolsky, W.T. Vetterling, B.P. Flannery : Numerical Recipes in FORTRAN 77: The Art of Scientific Computing. Cambridge University Press: Cambridge, (1992).